Journal of the Meteorological Society of Japan

EARLY ONLINE RELEASE

The DOI for this manuscript is
DOI:10.2151/jmsj.2021-025
J-STAGE Advance published date: January 13th, 2021

A case study of a quasi-stationary, very long Polar Stratospheric Cloud layer edge

Peter Voelger[1] and Peter Dalin[1]

[1] *Swedish Institute of Space Physics, Box 812, SE-981 28 Kiruna, Sweden*

Keywords: troposphere, stratosphere, polar stratospheric clouds, mountain gravity waves

Corresponding author: Peter Voelger (E-mail: peter.voelger@irf.se)

Abstract

A case study of occurrence of polar stratospheric clouds (PSCs) on February 13th, 2017 in northern Sweden is discussed in the present paper. For the first time a quasi-stationary edge of a bright and extended PSCs layer (~600 km long) on the Eastern side of the Scandinavian Mountain Range was photographed as well as registered with lidar observations. Both lidar measurements and model simulations demonstrated that atmospheric conditions were fairly unchanged for several hours during the presence of the PSC. Strong winds across the Scandinavian Mountain Range were responsible for triggering the formation of mountain lee waves in the Kiruna area, which in turn induced the formation of the quasi-stationary long and straight edge of the PSCs.

1. Introduction

Polar Stratospheric Clouds (PSCs) are a common phenomenon during Arctic and Antarctic wintertime. Their formation requires the stratospheric temperature to fall below ~ 195K (see e.g. Browell et al., 1990; Tabazadeh et al., 1994; Larsen et al., 1997). The formation temperature is usually only reached inside the polar vortex. Temperatures over the Arctic tend to be higher than over Antarctica since the Arctic vortex is more unstable. Therefore PSCs occur more frequently over Antarctica (Maturilli et al., 2005; Tilmes et al., 2006; Spang et al., 2016). This also means that

PSC formation in the Arctic is more strongly influenced by atmospheric disturbances such as waves (Carslaw et al., 1998; Kohma and Sato, 2011; Alexander et al., 2013). Sources for waves can be wind shear in the troposphere (e.g. the polar jet stream) or topographic features like ridges or mountain chains. One well-known, and well-documented source in Northern Europe is the Scandinavian Mountain Range (see e.g. Dörnbrack and Leutbecher, 2001; Blum et al., 2004; Kirkwood et al., 2010; Kaifler et al., 2017). Waves originating at the mountain range are known to produce temperature modulations due to vertical motion of air which allow the formation of PSCs at certain locations downstream (Voigt et al., 2000; Dörnbrack et al., 2002).

In an ideal case the uniform flow across a straight mountain ridge should result in a wave-like modulation of temperature downstream, with no variations parallel to the ridge. This would lead to long crests of clouds (see e.g. Fig, 16 of Fritts and Alexander, 2003). In reality clouds in the lee of the Scandinavian Mountain Range have more complex, patchy structures. Reasons are inhomogeneities in the horizontal wind field (horizontal wind shears), either due to local topographic effects or mesoscale variations. PSCs over Kiruna have been documented photographically for many years (see https://doi.org/10.34474/data.jmsj.133845**.v* and http://data.irf.se/data/dalin2020psc). Based on those observations it can be concluded that clouds with patchy structures are common over Kiruna, while well-defined cloud boundaries are a rare exception.

In the present paper we discuss an unusual case in which a PSC layer, that formed due to mountain lee waves, had an extended edge and remained stationary over a rather long period of time. In the following we will first explain the instruments and methods which are used in this study. Thereafter, the observations are described, followed by an interpretation and a summary.

2. Instruments and methods

This study is based on a combination of optical observations and model data. Photographic images were taken with a Canon G5 camera (resolution of 2592 x 1944 pixels) from the roof of the

main building of the Swedish Institute of Space Physics in Kiruna, Northern Sweden (IRF, located at 67.84°N, 20.41°E). Lidar measurements were performed with a backscatter lidar located at IRF. The lidar operates at a wavelength of 532 nm and has two detection channels to distinguish parallel and perpendicular polarisation of the backscattered light. The altitude range for observations is 5 to 50 km. Height and time resolution are 30 m and 133 s, respectively (see Voelger and Nikulin (2005) for more details).

For interpretation of atmospheric conditions during the period of interest, simulations with the Weather Research and Forecasting (WRF) model (Skamarock et al., 2008) were performed. WRF allows the calculation of the state of the atmosphere on a user-defined 3D grid for chosen time steps. As input for WRF we used ERA5 reanalysis data from the European Centre for Medium-Range Weather Forecasts (ECMWF). ERA5 data has a horizontal resolution of 31 km and 137 vertical levels (Hersbach et al., 2020).

3. Observational data

Images of a Polar Stratospheric Cloud were taken in Kiruna (67.84°N, 20.41°E) during the afternoon of February 13th, 2017 (Fig. 1). The cloud edge was unusual in that (a) it remained at the same location for several hours (at least during the period of visual and photographic observations 14-17 UT, corresponding to 15-18 LT) and (b) it was long and straight (modulated with filaments) along a line from southwest to northeast as long as about 600 km at least. Based on geographical features on the photographic images (e.g. mountains and the position of the sunset) it was possible to determine the angle between geographical north and cloud edge to be 44°±5° (Fig. 2). At the same time winds were consistently blowing from directions between north and northwest, hence approximately along the normal of the cloud edge. Wind speed at the ground was between 6 and 8 m/s as recorded by IRFôs weather station. Such wind conditions are favourable for the formation of mountain gravity waves on the lee side of the Scandinavian Mountain Range, i.e. on its eastern side. This strengthens the assumption that the cloud frontal shape is a result of mountain gravity waves.

During the following night IRFôs backscatter lidar was performing measurements 1 km south of the location where the photos were taken. The lidar operated from 17 UT until next morning 04:45 UT. Backscatter signals with both parallel and perpendicular polarisation were recorded. During the whole observation period a cloud layer was present in the stratosphere between 24 and 27 km altitude (Fig. 3). In lidar measurements PSCs can be characterized by (a) the depolarisation ratio $\breve{u} = I_{perp} / I_{par}$ with I being the measured backscatter intensity of the parallel and perpendicular channel, respectively, and (b) the backscatter ratio R, defined as $R = \left(\beta_{psc} + \beta_{mol}\right) / \beta_{mol}$ where β is the backscatter coefficient for PSCs and molecules, respectively. The combination of R and ŭ allows for the determination of the chemical composition of the cloud (see Browell et al., 1990 for details). In the case discussed here the combination of both large backscatter ratio and large depolarisation ratio indicated that the cloud consisted of ice particles. Over Northern Scandinavia such clouds most times only are formed in connection with mountain gravity waves (Blum et al., 2005).

4. Data Analysis

In order to put our local observations in a regional context we examined atmospheric conditions with help of WRF simulations. The model grid covered the northern part of Fennoscandia with 5.4 km distance between horizontal grid points and 160 height levels up to 10 hPa (see Fig. 2 for area covered by grid). Simulations were performed for a period of 96 hours, starting 48 hours before the photos were taken. Time resolution of output was set to 10 min.

Figure 4 shows simulated wind and temperature fields at 25 km altitude for times 12 and 18 UT on date 13/02/17 and at 00 UT on date 14/02/17, as derived with WRF. During all three times wind directions north of 65°N were roughly perpendicular to the Scandinavian Mountain Range. Both wind speed and direction changed only marginally during this period. The wind field induced a wavelike horizontal quasi-stationary motion which resulted in a perturbation of the temperature field above and in the lee of the mountains. The position and orientation of the main temperature

minimum just behind the mountains corresponds well to the position of the PSC edge at 12 UT and 18 UT on February 13th, 2017. The orientation of the temperature minimum at 00 UT on February 14th corresponds less to the orientation of the PSC edge. Visual observation of the development of the cloud edge was not possible at that time of the day due to darkness. However, our lidar observations proved the continuing presence of a PSC layer. Additionally, the spaceborne lidar CALIOP detected a PSC at approximately 69°N, 29°E while passing the Gulf of Bothnia east of Kiruna during that night, shortly after 01 UT.

A commonly used indicator for the vertical stratification of the atmosphere is the buoyancy frequency, *N*, also called the Brunt-Väisälä frequency (see e.g. Holton, 1992). Figure 5 illustrates a cross section of *N* through the location of the ground-based observations and along the wind direction at 18 UT. One can see that the first positive maximum is observed right above the mountains at about 2 km, then other maxima occur at 14, 27-28, 37-39 km altitudes, hence a vertical wavelength of the main mountain wave is about 10-12 km above the Kiruna area. The upward direction of energy propagation can be seen from the vertical phase propagation directed downward relative to the mean flow (which is from the left to right in Figure 5) and westward relative to the mountains (Holton, 1992). Two buoyancy minima at 5 and 10 km as well as two maxima at 14 and 28 km are directed westward relative to the mountain ridge and with height. These phase tilts provide the evidence of the upward wave energy propagation as expected since the energy source for these waves was located at the ground (mountains).

Figure 6 shows the temporal development of the buoyancy frequency near the mountain crest at 69°N, 19°E (left panel) and in the lee of the mountains at 67.84°N, 20.41°E (right panel). Here, WRF was used to achieve better time resolution than with ERA5. At both locations vertical profiles of *N* remained fairly unchanged for about 24 hours showing wave-like structures. In Fig. 7 a profile for the buoyancy frequency near the mountain crest is displayed. While some temporal variation of absolute numbers does occur, the height of the features varies only marginally. Estimating the vertical length of the wave-like motion is straight forward. It was in the range of 10-12 km, both

above the mountain range and in the lee of the mountains where both photos were taken and lidar measurements were performed.

An apparently stationary wave in the lee of a mountain is a special case of a topographic wave (see e.g. Holton, 1992). For a wave to appear to be stationary its phase speed *c* has to be exactly the opposite of the speed of the mean flow $\overline{u}$. The dispersion relation for a stationary wave is then

$$0 = \overline{u} \pm \frac{N}{\sqrt{k^2 + m^2}} \qquad (1)$$

Here, *N* is the buoyancy frequency, *k* and *m* are horizontal and vertical wavenumber, respectively. Note that Figure 4 demonstrates the background wind which is quasi perpendicular to the PSC edge hence is almost parallel to the *k* vector. The equation can be simplified to

$$m^2 = \frac{N^2}{\overline{u}^2} - k^2 \qquad (2)$$

In our case the horizontal wavelength is longer than 200 km as one can see in Figure 4, hence $k < N / \overline{u}$. For a wave with a vertical wavelength of 12 km to be created the horizontal wind speed needs to be ~40 m/s. This means that the stationary wave was created at an altitude range where horizontal wind speed is around that value, i.e. in the lower troposphere right above the mountains as demonstrated in Fig. 8. Figure 8 illustrates that the horizontal wind speed was varying around 40 m/s in the range of 35-45 m/s between 2 and 15 km. Small amplitude modulations of the mean wind speed between 5 and 15 km are also seen due to interference with small-scale gravity waves. These small-scale modulations are also reproduced in the buoyancy frequency between 6 and 13 km seen in Fig. 7. Since the vertical wavelength *m* is a function of both the buoyancy frequency and mean wind speed (see Eq. 2), *m* might slightly change due to these small variations. However, the main period of the vertical wavelength of 10-12 km is unchanged and is clearly seen both in the buoyancy frequency (Fig. 7) and in the horizontal wind speed (Fig. 8) between 3 and 13 km. Note that the horizontal wind speed, along the horizontal wavenumber vector, does not approach to zero meaning that there were no any critical levels for mountain gravity waves propagating from the ground to the PSC altitude. The created mountain wave induced its own variations on the horizontal

wind speed, resulting in high variations in the horizontal wind speed at higher altitudes above 15 km, with maximum wind speed changes of ~40 m/s at the 30 km altitude. Thus, theoretical considerations fit to WRF model wind data that confirm a principal possibility of the formation of a stationary gravity wave above and in the lee of the mountains.

5. Summary

For the first time, a quasi-stationary very long (~600 km) and nearly straight Polar Stratospheric Cloud edge was observed in Kiruna, Northern Sweden on February 13th, 2017. Both lidar observations and simulations with WRF showed that atmospheric conditions were fairly unchanged for several hours. At the same time strong winds across the Scandinavian Mountain Range were present which triggered the formation of mountain lee waves in the Kiruna area. It was shown that the stationary waves that could be observed were formed by horizontal winds with 40 m/s wind speed. Such wind speeds were found in the lower troposphere at about 3 km altitude. Hence, the waves that created the stationary cloud edge in the stratosphere propagated upwards from the lower troposphere.

Acknowledgment

This study was conducted using resources provided by the Swedish National Infrastructure for Computing (SNIC) at the High Performance Computing Center North (HPC2N), Umeå University, Sweden. The observation data (PSC images and lidar measurements) related to this article can be found at https://doi.org/10.34474/data.jmsj.133845**.v* and the project ftp server: ftp://ftp.irf.se/outgoing/pdalin/PSC_2017/.

178 **References**

179 Alexander, S. P., A. R. Klekociuk, A. J. McDonald, and M. C. Pitts, 2013: Quantifying the role
180 of orographic gravity waves on polar stratospheric cloud occurrence in the Antarctic and the Arctic.
181 *J. Geophys. Res.*, **118**, 11493-11507, doi:10.1002/2013JD020122.
182 Blum, U., K. H. Fricke, G. Baumgarten, and A. Schöch, 2004: Simultaneous lidar observations
183 of temperatures and waves in the middle atmosphere on the east and west side of the Scandinavian
184 Mountains: a case study on 19/20 January 2003. *Atmos. Chem. Phys.*, **4**, 809-816, doi:1680-
185 7324/acp/2004ï 4-809.
186 Blum, U., K. H. Fricke, K. P. Mueller, J. Siebert, and G. Baumgarten, 2005: Long-term lidar
187 observations of polar stratospheric clouds at Esrange in northern Sweden. *Tellus*, **B57**, 412-422,
188 doi:10.3402/tellusb.v57i5.16562.
189 Browell, E. V., C. F. Butler, S. Ismail, P. A. Robinette, A. F. Carter, N. S. Higdon, O. B. Toon,
190 M. R. Schoeberl, and A. F. Tuck, 1990: Airborne lidar observations in the wintertime arctic
191 stratosphere: Polar stratospheric clouds. *Geophys. Res. Lett.*, **17**, 385-388.
192 Carslaw, K. S., M. Wirth, A. Tsias, B. P. Luo, A. Dörnbrack, M. Leutbecher, H. Volkert, W.
193 Renger, J. T. Bacmeister, E. Reimer, and Th. Peter, 1998: Increased stratospheric ozone depletion
194 due to mountain-induced atmospheric waves. *Nature*, **391**, 675-678.
195 Dörnbrack, A., T. Birner, A. Fix, H. Flentje, A. Meister, H. Schmid, E. V. Browell, and M. J.
196 Mahoney, 2002: Evidence for inertia gravity waves forming polar stratospheric clouds over
197 Scandinavia. *J. Geophys. Res.*, **107D**, doi:10.1029/2001JD000452.
198 Dörnbrack, A., and M. Leutbecher, 2001: Relevance of mountain waves for the formation of
199 polar stratospheric clouds over Scandinavia: a 20 year climatology. *J. Geophys. Res.*, **106**, 1583-
200 1593.
201 Fritts, D. C., M. J. Alexander, 2003: Gravity waves dynamics and effects in the middle
202 atmosphere. Rev. Geophys., **41**, doi:10.1029/2001RG000106.
203 Hanson, D., K. Maurenberger, 1988: Laboratory studies of the natric acid trihydrate:
204 Implications for the south polar stratosphere, Geophys. Res. Lett., **15**, 855-858.
205 Hersbach, H., B. Bell., P. Berrisford, S. Hirahara, A. Horányi, J. Muñoz-Sabater, J. Nicolas, C.
206 Peubey, R. Radu, D. Schepers, A. Simmons, C. Soci, S. Abdalla, X. Abellan, G. Balsamo, P.
207 Bechtold, G. Biavati, J. Bidlot, M. Bonavita, G. De Chiara, P. Dahlgren, D. Dee, M. Diamantakis,
208 R. Dragani, J. Flemming, R. Forbes, M. Fuentes, A. Geer, L. Halmberger, S. Healy, R. J. Hogan, E.
209 Hólm, M. Janisková, S. Keeley, P. Laloyaux, P. Lopez, C. Lupu, G. Radnoti, P. de Rosnay, I.
210 Rozum, F. Vamborg, S. Villaume, and J.-N. Thépaut, 2020: The ERA5 global reanalysis. Q. J. R.
211 Meteorol. Soc., **146**, 1999-2049, doi: 10.1002/qj.3803.
212 Holton, J. R., 1992: An introduction to dynamic meteorology. *Academic Press*, San Diego, 507

pp.

Kaifler, N., B. Kaifler, B. Ehard, S. Gisinger, A. Dörnbrack, M. Rapp, R. Kivi, A. Kozlovsky, M. Lester, and B. Liley, 2017: Observational indications of downward-propagating gravity waves in middle atmosphere lidar data. *J. Atmos. Sol.-Terr. Phys.*, **162**, 16-27, doi:10.1016/j.jastp2017.03.003.

Kirkwood, S., M. Mihalikova, T. N. Rao, and K. Satheesan, 2010: Turbulence associated with mountain waves over Northern Scandinavia ï a case study using ESRAD VHF radar and the WRF mesoscale model. *Atmos. Chem. Phys.*, **10**, 3583-3599, doi:10.5194/acpd-10-3583-2010.

Kohma, M and K. Sato, 2011: The effects of atmospheric waves on the amounts of polar stratospheric clouds. *Atmos. Chem. Phys.*, **11**, 11535-11552, doi:10.5194/acp-11-11535-2011.

Larsen, N., B. M. Knudsen, J. M. Rosen, N. T. Kjome, R. Neuber, and E. Kyrö, 1997: Temperature histories in liquid and solid polar stratospheric cloud formation. *J. Geophys. Res.* **102D**, doi:10.1029/97JD01666.

Marti, J., K. Mauersberger, 1993: A survey and new measurements of ice vapor pressure at temperatures between 170 and 250K, Geophys. Res. Lett., **20**, 363-366.

Maturilli, M., R. Neuber, P. Massoli, F. Cairo, A. Adriani, M. L. Moriconi, and G. Di Donfrancesco, 2005: Differences in Arctic and Antarctic PSC occurrence as observed by lidar in Ny-Ålesund (79ºN, 12ºE) and McMurdo (78ºS, 167ºE). *Atm. Chem. Phys.*, **5**, 2081-2090.

Skamarock, W. C., J. B. Klemp, J. Dudhia, D. O. Gill, D. M. Barker, M. G. Duda, X.-Y. Huang, W. Wang, and J. G. Powers, 2008: A description of the advanced research WRF version 3. *NCAR Tech. Note*, NCA170213_depol_nightR/TN-475+STR, 113 pp, doi:10.5065/D68S4MVH.

Spang, R., L. Hoffmann, M. Höpfner, S. Griessbach, R. Müller, M. C. Pitts, A. M. W. Orr, and M. Riese, 2016: A multi-wavelength classification method for polar stratospheric cloud types using infrared limb spectra. *Atmos. Meas. Tech.*, **9**, 3619-3639.

Tabazadeh, A., R. P. Turco, K. Drdla, M. Z. Jacobson, and O. B. Toon, 1994: A study of type I polar stratospheric cloud formation. *Geophys. Res. Lett.*, **21**, 1619-1622.

Tilmes, S., R. Müller, A. Engel, M. Rex, and J. M. Russell, 2006: Chemical ozone loss in the Arctic and Antarctic stratosphere between 1992 and 2005. *Geophys. Res. Lett.*, **33**, doi:10.1029/2006GL026925.

Voelger, P. and G. Nikulin, 2005: The new lidar system at the Swedish Institute of Space Physics in Kiruna: description and first measurements. *ESA SP-590*, 321-325.

Voigt, C., A. Tsias, A. Dörnbrack, S. Mellinger, B. Luo, J. Schreiner, N. Larsen, K. Mauersberger, and T. Peter, 2000: Non-equilibrium compositions of liquid polar stratospheric clouds in gravity waves. *Geophys. Res. Lett.*, **27**, 3873-3876.

Figure captions:

Fig. 1. Photos of PSC in WSW direction (left) and ENE direction (right), taken on February 13th, 2017 at 14:31 UT and 16:08 UT, respectively, in Kiruna (Sweden).

Fig. 2. Estimated front of the observed PSC based on sunset and on identification of topographic features that are visible in the photos in Fig. 1. Thin black lines mark the edges of the grid used in WRF simulations.

Fig. 3. Backscatter ratio (BSR) from lidar observations of the PSC layer as the function of time and intensity on 13-14 February 2017. The backscatter signal in the parallel polarization channel is shown.

Fig. 4. Horizontal maps of the wind velocity with wind vectors (left side) and temperature (right side) fields at 25 km altitude for times 12 UT, 18 UT on February 13th and 00 UT on February 14th as calculated by WRF. The black line (same as blue line in Fig. 2) marks the edge of the observed PSC. White lines indicate the existence temperatures for NAT particles (solid, Hanson and Mauersberger, 1988) and ice particles (dashed, Marti and Mauersberger, 1993).

Fig. 5. Buoyancy frequency variations calculated from ERA5 data as a function of the geographical position through the observational point along the horizontal wind direction and altitude at 18 UT on February 13th 2017. The horizontal axis gives the geographical coordinates along the cross section parallel to horizontal wind direction. The vertical white line shows the position of the lidar observational point. The height profile of the Scandinavian Mountain Range along the cross section is shown in white at the bottom of the figure. The arrow indicates the direction of the horizontal wind.

Fig. 6. Buoyancy frequency as a function of time as calculated with WRF. Left: near the mountain crest, right: at location of lidar observations.

Fig. 7. Profile of buoyancy frequency derived as calculated with WRF for a location near the mountain crest.

Fig. 8. Profile of horizontal wind speed perpendicular to the mountain crest (background horizontal wind along the horizontal wavenumber vector) as calculated with WRF. The location of the profile is near the mountain crest.

Figures

Figure 1.

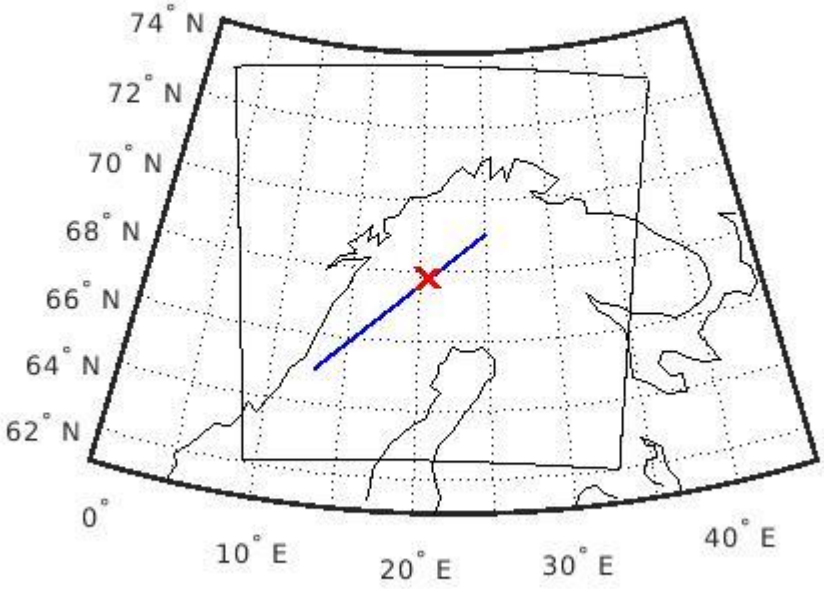

285

286 **Figure 2**.

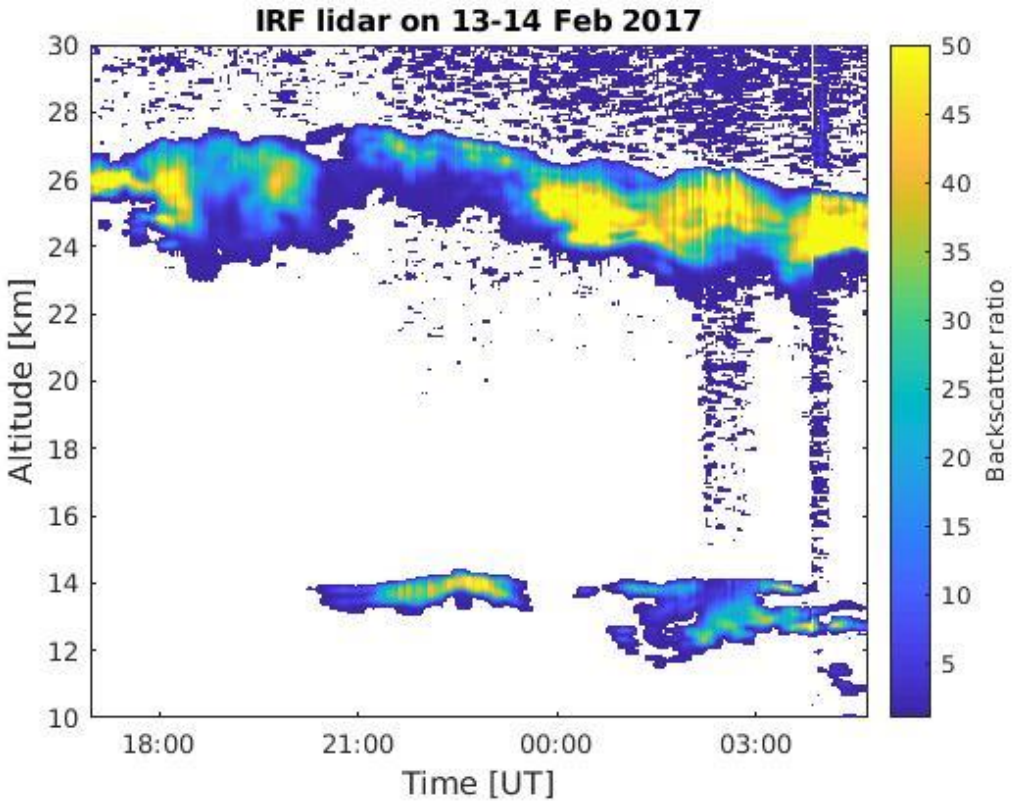
IRF lidar on 13-14 Feb 2017
Altitude [km]
30
28
26
24
22
20
18
16
14
12
10
18:00
21:00
00:00
03:00
Time [UT]
50
45
40
35
30
25
20
15
10
5
Backscatter ratio

Figure 3.

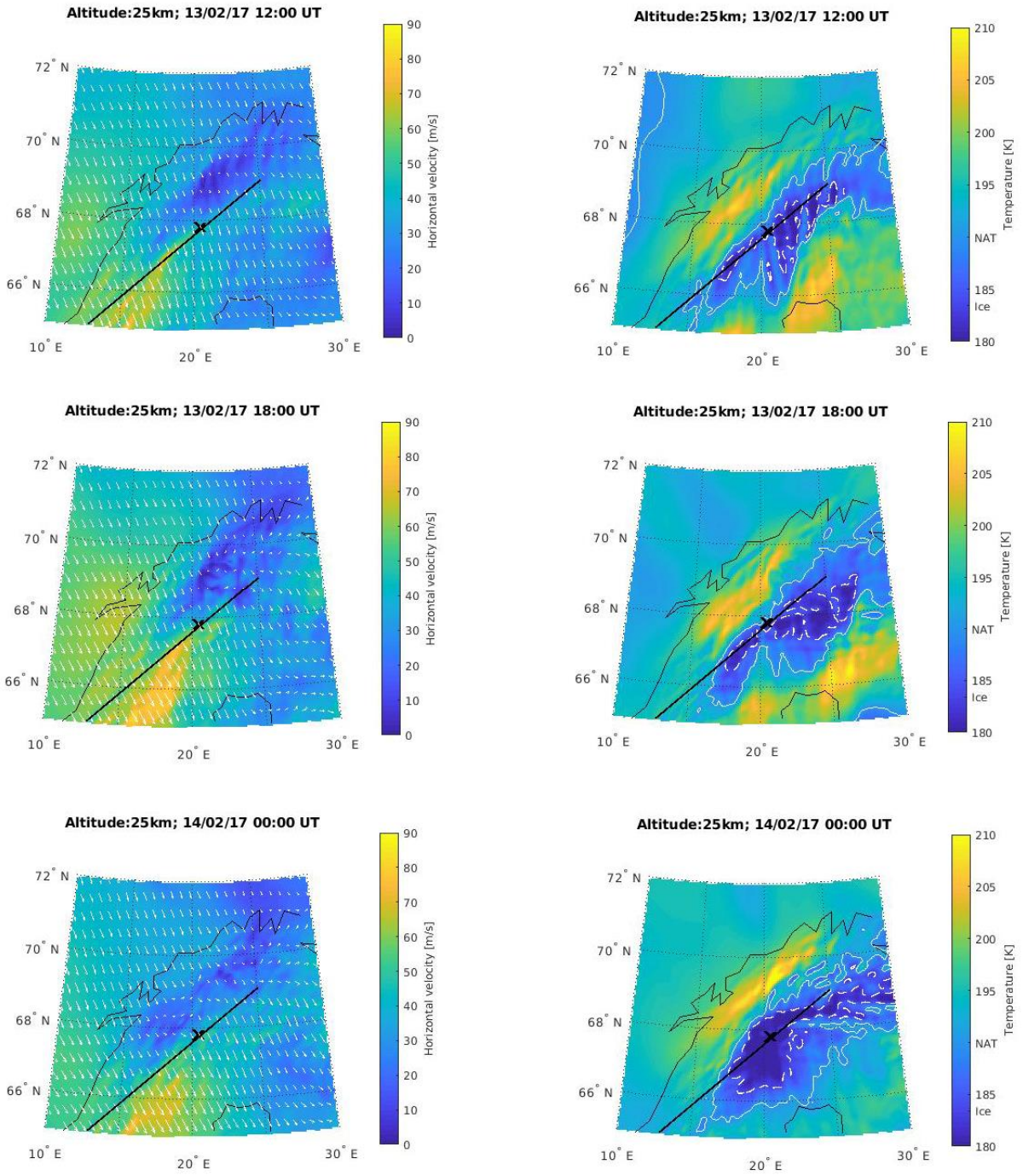

289

290 **Figure 4.**

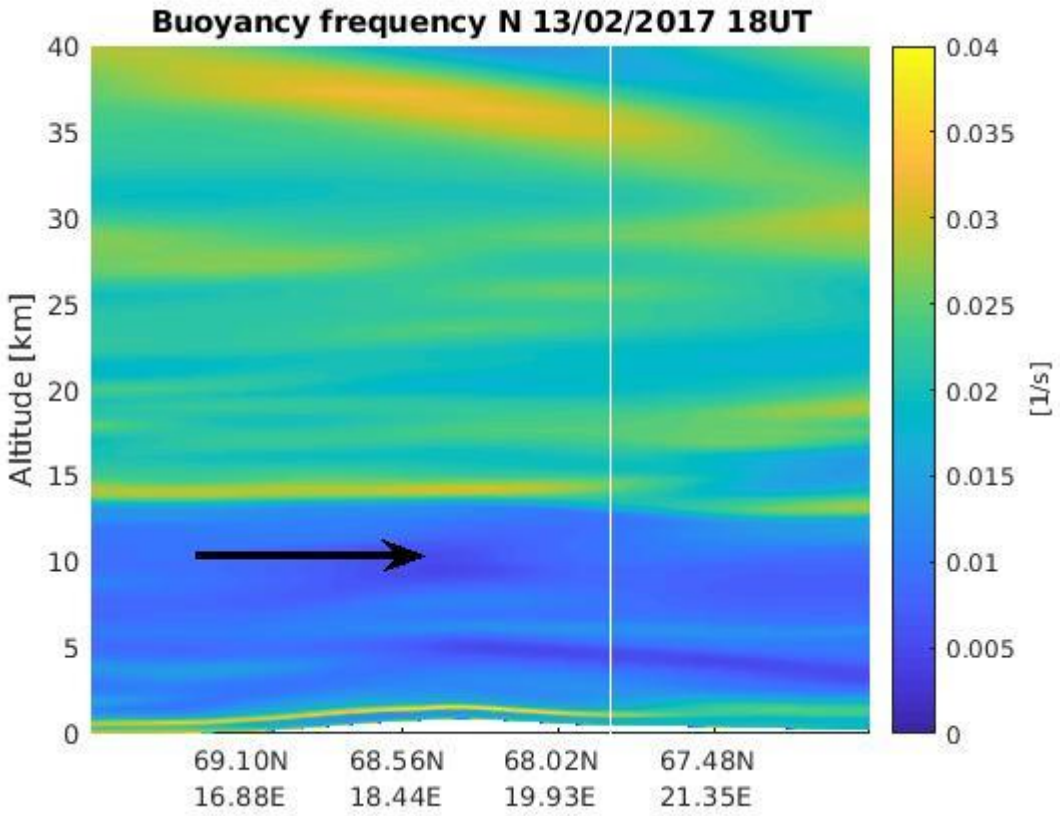

291

292 **Figure 5**.

293

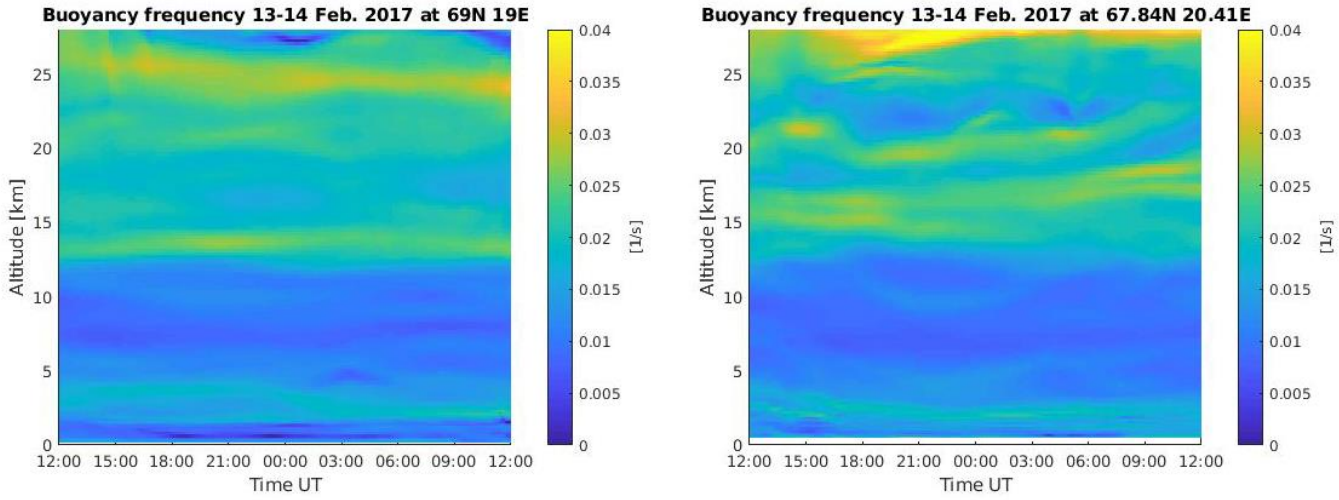

294

295 **Figure 6**.

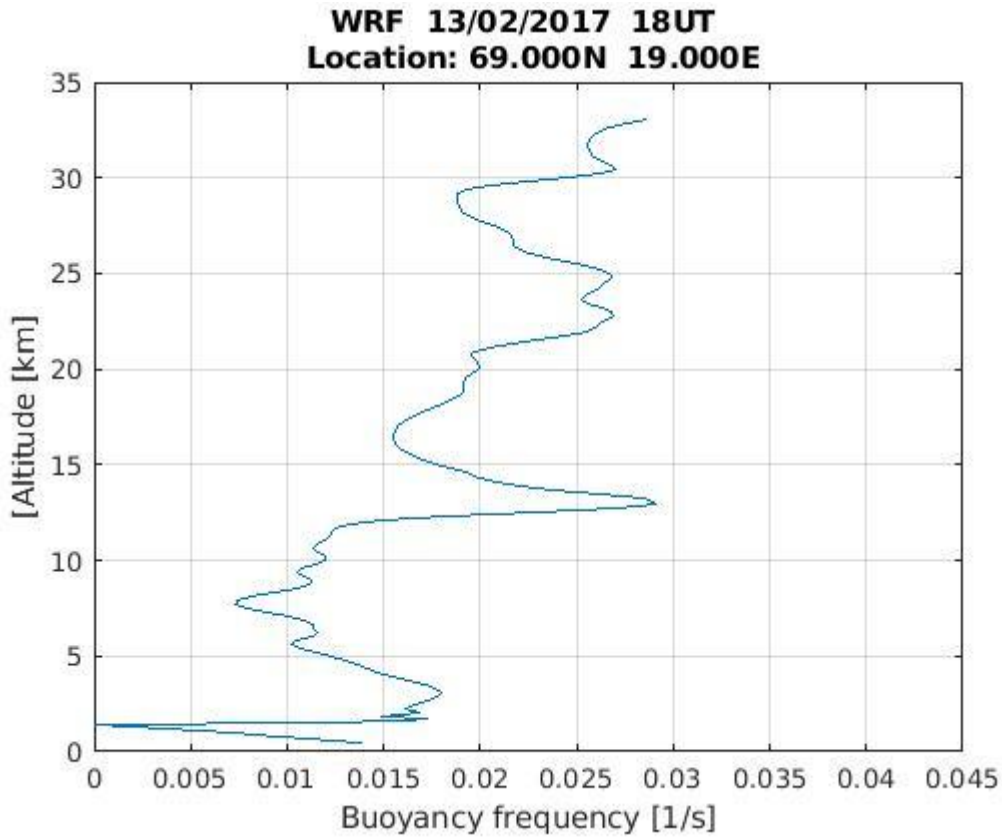

296

297 **Figure 7**.

298

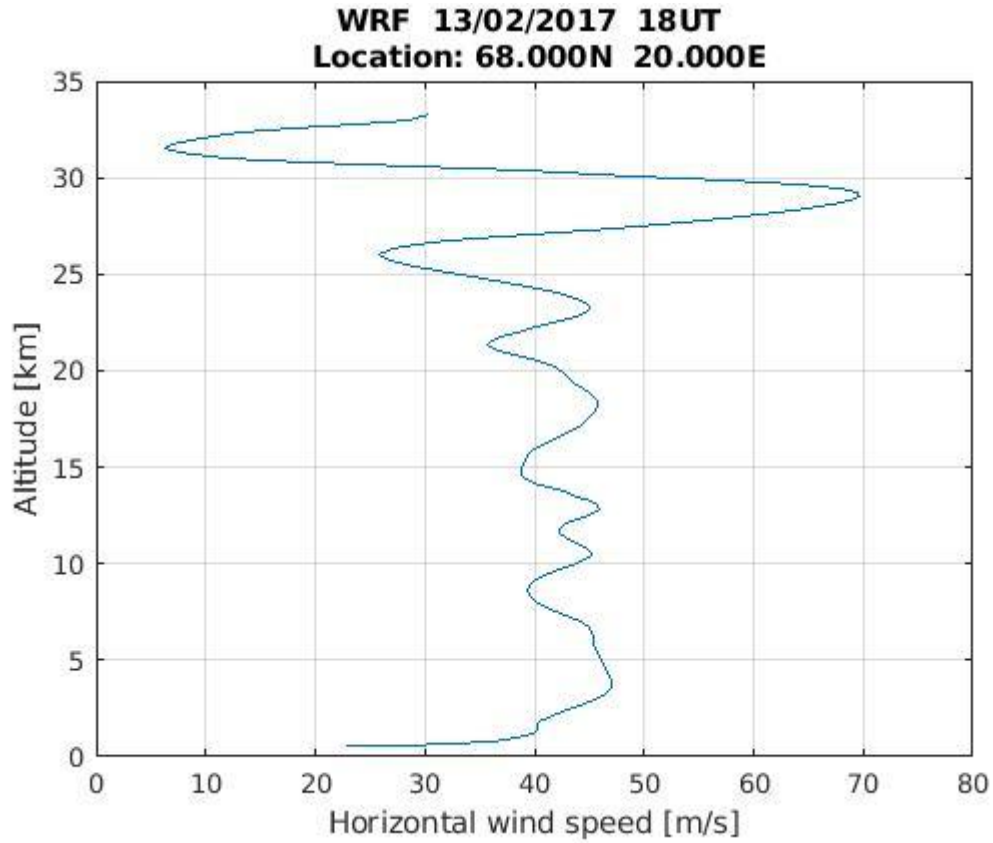

299

300 **Figure 8**.

301